Langevin simulation of rf collisional multipactor breakdown of gases

L. Conde,[1] F. Pérez,[2] J. de Lara,[3] M. Alfonseca,[3] and D. Raboso[4]
[1]*Departamento de Física Aplicada, E.T.S.I. Aeronáuticos, Universidad Politécnica de Madrid, 28040 Madrid, Spain*
[2]*GMV, Isaac Newton 11, Tres Cantos, E28760 Madrid, Spain*
[3]*E.T.S. Informática, Universidad Autónoma de Madrid, 28049 Madrid, Spain*
[4]*ESA/ESTEC, Keplerplaan 1, Postbus 299, 2200 AG Noordwijk, The Netherlands*
(Received 12 February 2009; published 16 June 2009)

The thresholds for the electron multiplication in both multipactor and the so-called collisional multipactor microwave discharges are calculated by means of an individual particle model. The simulations are restricted to low and intermediate gas pressures, where the collisional mean-free path of electrons is of the same order or larger than the characteristic dimension of the system. Thus, the charge multiplication is caused by both the electron impact ionization of the neutral gas and the secondary electron emission by electron collisions at the surfaces. The charge avalanche is simulated by the numerical integration of the trajectories of electrons up to the characteristic time for the space-charge buildup. The electron dynamics is described by the stochastic Langevin equations where the collisional scatter of electrons is incorporated by means of a random force, while the microwave electric field and the friction are deterministic forces. The physical properties of materials at the walls are considered by means of realistic models deduced from experimental data fitting, while the constant collision frequency model is used for elastic and inelastic electron collisions with neutral atoms. Previous results for low pressure electron multipactor are recovered, and for pressures corresponding to collisional multipactor the predictions of this simple model are in agreement with both the experimental results and particle in cell and Monte Carlo simulations. Finally, physical conditions under which the charge multiplication develops and the limitations for higher pressures of the proposed model are also discussed.

DOI: 10.1103/PhysRevE.79.066403 PACS number(s): 52.80.Pi

I. INTRODUCTION

The prediction of the radio frequency (rf) electric breakdown thresholds is of paramount importance for the design of microwave systems [1], particle accelerators [2], or in semiconductor processing [3]. The charge avalanche dissipates an important fraction of the rf input power and may eventually lead to the catastrophic failure of the system. The numerical simulations of the rf discharge buildup save expensive laboratory testing and also make it possible to predict their material-dependent performances.

Two different charge production processes contribute to the rf breakdown. First, the electron impact ionization of the neutral gas in the open spaces of the microwave devices by free electrons accelerated by the rf electric field. In second place, the collision of these energized electrons with the walls of the equipment may also produce additional charges by secondary electron emission. The weight of each charge production mechanism depends on the local neutral pressure p_a, the magnitude of the rf electric field and the properties of the materials used for the microwave components.

For very low pressures, roughly below 10^{-4} mbars, the contribution of collisional ionization is negligible. The mean-free path for elastic collisions between electrons and neutral atoms λ_{ea} is much larger than the characteristic dimension D of waveguides, which is on the order of a few centimeters. Furthermore, the electrons that collide against the walls may be absorbed, reflected back, or give rise to the release of additional secondary electrons.

The low pressure electron avalanche essentially depends on the secondary electron emission coefficient of the surfaces. This material-dependent rf breakdown is the denominated *multipactor* (MP) and has been thoroughly studied for different geometries with both metallic [4–7] and dielectric surfaces [4,8–11].

The thresholds for multipactor are predicted by means of a resonance condition between the electron time of flight and the rf electric field cycle that produces a new secondary electron at each electron impact at the walls [4–6]. The thresholds for multipactor between two parallel walls [4–7] and also along a single surface [4,10,11] have been successfully calculated by these resonant electron models. In addition, the buildup and the time evolution of this electron discharge have been studied using particle in cell (PIC) and Monte Carlo (MC) schemes [10,11] and more recently by single-electron tracking simulations [12].

At the opposite high pressure limit (roughly over 10^{-1} mbar), where $D \gg \lambda_{ea}$, the charge transport toward the walls is hindered by collisions with neutral gas atoms. The gas pressure p_a is proportional to the electron collision frequency for momentum transfer with neutrals $p_a \sim \nu_m$ over the involved microwave frequencies $f_w < \nu_m$. This restricted electron motion leads to a negligible rate of secondary electron production at the walls and the collisional ionization becomes the relevant charge production process. The classical Paschen curves predict the thresholds for these charge avalanches, which produce plasmas of ions and electrons [13,14]. The time evolution of this electric breakdown has also been simulated by PIC techniques [15] as well as by means of more involved kinetic models [16].

However, both charge production processes coexist for the intermediate pressure range of $p_a \simeq 10^{-3}-10^{-1}$ mbar, as evidenced by the complex variation in the rf breakdown voltages with the neutral gas pressure found in the experimental data [17]. In this case the collisional mean-free path of elec-

trons is similar to the characteristic length $D \simeq \lambda_{ea}$ and the collision frequencies (between $\sim 10^{-2}$ and 1.0 GHz) are similar to $f_w \sim \nu_m$.

This rf electric breakdown at intermediate pressures has been called *multipactor plasma* [17] or *collisional multipactor* (CMP) [18–20]. The CMP charge avalanche is more complex than the pure electron MP because of the random electron collisions. Therefore, the resonant conditions for MP electron multiplication are no longer valid.

More involved formulations have been proposed to account for the electron collisions in resonant electron models for CMP [18–20]. First, the electron impact ionization is neglected under the assumption that the energy acquired by the electron always lies below the ionization energy of the neutral gas [18]. Alternatively, the number of electrons originated by collisional ionization is small compared with the secondary electron production rate [19]. For higher electron energies, a modified MP breakdown condition has been proposed which considers that a fraction of the electrons born by collisional ionization become a part of the multipacting resonant electron group [20]. In addition, the CMP charge multiplication process has also been simulated by means of PIC and MC schemes [21,22].

Recently, the MP breakdown thresholds have been accurately predicted by using an individual particle tracking model where the motion of up to 2×10^4 individual electrons were simultaneously considered [12]. In this paper, this single-particle tracking scheme is extended to account for both the elastic and the ionizing collisions of electrons in order to predict the thresholds for CMP breakdown. The stochastic Langevin equations of motion model the collisional trajectories of electrons driven by the rf electric field. These equations have also been formulated to account for the Coulomb collisions in PIC schemes [23–25] and similar direct particle simulations have been employed to simulate the streamer initiation processes [26,27].

As we shall see, this simple model leads to acceptable predictions of the CMP rf breakdown thresholds which are compared with the experimental data of Ref. [17]. In addition, the previous results for MP breakdown of Ref. [12] are recovered in the limit for low neutral gas pressures.

Section II of his paper discusses the geometry and the approximations of our model. The Langevin equations of motion for electrons are introduced in Sec. III. The numerical scheme as well as the limitations of our simulations is discussed in Sec. IV. The obtained numerical results and a comparison with experimental data are presented in Sec. V. Finally we end with some concluding remarks.

II. TIME SCALES AND MODEL APPROXIMATIONS

The geometry of the present model is shown in Fig. 1 and consists of two coated parallel plates P and P', separated by a distance D, with equal areas $A=S \times H$. The sinusoidal rf wave with frequency $\omega=2\pi f_w$ propagates along the Z axis and creates a time varying electric field $E_w(t)=E_{ox} \sin(\omega t)$ directed along the X axis with an amplitude $E_{ox}=(V_o/D)$.

The typical rf peak voltages are high, in the range $V_o \simeq 10^2-10^3$ volts and the microwave frequencies lie between

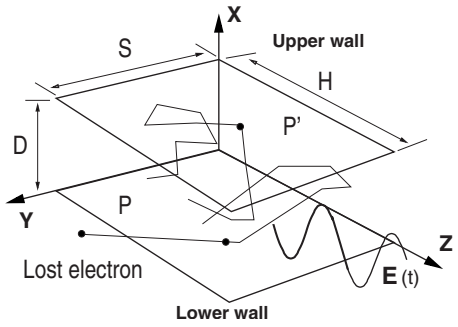

FIG. 1. The model geometry with the lower (P) and upper (P') coated surfaces separated by the gap height D.

0.1 and 35.0 GHz. This covers most of the bandwidths employed for space applications called C, X, Ku, and Ka. For the involved gas pressures the neutral atom densities are several orders of magnitude ($n_a \simeq 10^{12}-10^{14}$ cm^{-3}) above the maximum number of individual electrons (2×10^4) employed in the simulations. Therefore a uniform neutral atom background will be considered in the following.

As in previous models for MP and CMP, the scope of these simulations is restricted up to the characteristic time T_d for the space-charge buildup [7,18–20]. Below this time scale, the local electric field $\mathbf{E}_l$ created by the free charges within the volume V_s is small compared with the microwave electric field $|\mathbf{E}_w| \geqslant |\mathbf{E}_l|$ [21–28].

In the present model, this maximum simulation time scale is fixed as in PIC simulations, where the characteristic time found is $T_b < 2 \times 10^{-6}$ s for pressures in the CMP range between 1.3×10^{-3} and 6.7×10^{-2} mbar [21,28]. This represents a conservative upper bound, compared with typical breakdown times found in the experiments for pressures over 1 mbar, which are below 25 ns [29]. Therefore, as in previous simulations, the space-charge effects are neglected during 2×10^2 up to 7×10^4 periods of the involved microwave frequencies.

In addition, the contribution during T_b to the local electric field $\mathbf{E}_l$ of ions produced by collisional ionization is also neglected [7,18–20]. Heavy ions experience elastic and charge exchange collisions with neutrals where no additional particles are originated. Besides, the number of new charges produced by ions impacting the walls is very small compared with the secondary electron emission rate.

The new electrons are created by either electron impact ionization of gas atoms or by secondary electron emission at the walls. The details for the electron interaction with the coated surfaces at the walls are already described in Ref. [12]. Additional electron losses by volume recombination and electron attachment are neglected, because the corresponding mean-free paths exceed by orders of magnitude the typical dimensions of microwave devices.

III. LANGEVIN EQUATIONS FOR ELECTRONS

The electrons are accelerated by the deterministic force of the microwave electric field $\mathbf{F}_{el} \simeq -e\mathbf{E}_w(t)$ and are also randomly scattered by the elastic collisions with the neutral at-

oms. Two forces acting on electrons, $\mathbf{F}_r$ and $\mathbf{F}_s$, account for this collisional interaction. The friction force

$$\mathbf{F}_r = -m_e \nu_m \mathbf{u}_e \tag{3.1}$$

represents the resistance to the electron advance along the direction parallel to its speed $\mathbf{u}_e$ [18–20]. The change in the direction of the electron speed caused by elastic collisions with neutrals is introduced by means of the time-dependent random force

$$\mathbf{F}_s = \mathbf{C} \cdot \mathbf{\Gamma}(t), \tag{3.2}$$

which couples the random components of the vector $\mathbf{\Gamma}(t)$ through the elements of the matrix $\mathbf{C}$ [23–25,30]. Because two successive collision events are uncorrelated, the components $\Gamma_i(t)$ satisfy

$$\langle \Gamma_i(t) \rangle = 0,$$

$$\langle \Gamma_i(t) \Gamma_j(t') \rangle = \delta_{ij} \delta(t - t'),$$

where suffixes $i,j=x,y,x$ denote the spatial coordinates [23–25].

The density of neutrals $n_a \gg n_e$ is uniform within V_s and $\mathbf{E}_w(t)$ changes in time; therefore, there is no privileged direction for the collisional scattering of electrons. Thus, the matrix $\mathbf{C}$ is diagonal with $C_{ii}=C$ and

$$C = \sqrt{\frac{2K_B T_e}{m_e}} \sqrt{\nu_m}, \tag{3.3}$$

which depends on ν_m and the electron temperature $K_B T_e$ [23–25].

Finally, the involved cross sections are approximated by averaged energy-independent values leading to constant collision frequencies $\nu_m = n_a \sigma_m u_r$ and $\nu_I = n_a \sigma_I u_r$ in Eqs. (3.1) and (3.3). The characteristic speed $u_r = \sqrt{2eV_r/m_e}$ is related with the rms value $V_r = V_o/\sqrt{2}$ of the microwave peak amplitude. This approximation neglects the low-energy effects in the collision cross section because of the large values of V_o.

The following system of stochastic differential equations models the motion of the electrons present in the test volume of Fig. 1:

$$\frac{d\mathbf{r}_e}{dt} = \mathbf{u}_e, \tag{3.4}$$

$$\frac{d\mathbf{u}_e}{dt} = -\frac{e}{m_e}\mathbf{E}(t) - \nu_m \mathbf{u}_e + \mathbf{C} \cdot \mathbf{\Gamma}(t). \tag{3.5}$$

In this context, these Langevin equations of motion have been previously employed to model the Coulomb collisions in PIC codes [23,24], the dynamics of charged particle beams [25], the electron runaway in a plasma [30], or the Brownian motion of charged particles in dusty plasmas [31].

Equations (3.4) and (3.5) are made dimensionless by using the waveguide gap D for the length scale and the period of the rf wave $\tau = t/T_w$, where $T = 1/f_w$ for the time scale. Thus, $d/dt = f_w d/d\tau$ and $p = x/D$, $q = y/D$, $r = z/D$ are the dimensionless coordinates and U_p, U_q, and U_r the corresponding speeds. Therefore,

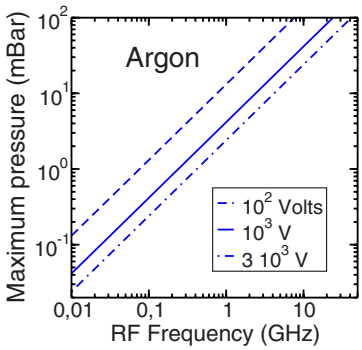

FIG. 2. (Color online) The maximum simulation pressures and different microwave peak amplitudes V_o for argon with $N_s = 200$.

$$\frac{dU_p}{d\tau} = -\frac{\nu_m}{f_w} U_p - \frac{1}{2}\left(\frac{V_m}{D f_w}\right)^2 \sin(2\pi\tau) + \frac{V_{Te}}{D f_w}\sqrt{\frac{\nu_m}{f_w}}\zeta_p(\tau), \tag{3.6}$$

$$\frac{dU_q}{d\tau} = -\frac{\nu_m}{f_w} U_q + \frac{V_{Te}}{D f_w}\sqrt{\frac{\nu_m}{f_w}}\zeta_q(\tau), \tag{3.7}$$

$$\frac{dU_r}{d\tau} = -\frac{\nu_m}{f_w} U_r + \frac{V_{Te}}{D f_w}\sqrt{\frac{\nu_m}{f_w}}\zeta_r(\tau), \tag{3.8}$$

where $V_{Te} = \sqrt{2K_B T_e/m_e}$ and $V_m^2 = 2eV_o/m_e$.

Equations (3.7) and (3.8) govern the electron motion along the Y and Z directions in Fig. 1, while Eq. (3.6) gives the rf sinusoidal electric field along the X coordinate. The continuous time-dependent quantities $\zeta_p(\tau)$, $\zeta_q(\tau)$, and $\zeta_r(\tau)$ are dimensionless Gaussian random variables.

In Eqs. (3.6)–(3.8) the relative weight of each term depends on the ratio ν_m/f_w, the rf voltage peak amplitude V_o, and the waveguide gap length D. In the limit $\nu_m/f_w \ll 1$, both the friction terms and the random force $\mathbf{F}_s$ become negligible and then the collisionless electron motion is only driven by the deterministic force of the microwave electric field.

IV. NUMERICAL SCHEME

The collisional interaction of electrons with the neutral gas atom background is incorporated by means of the random path needed for the numerical integration of Eqs. (3.6)–(3.8) using a Milstein scheme. After a small integration time interval $\Delta\tau$, the calculation of the dimensionless position and velocity of each electron requires the evaluation of a Brownian path with $0 \le \nu_m/f_w \le N_s$ substeps [32]. The maximum number $N_s = T_w/\tau_c$ of time subintervals is determined by the minimum average time τ_c considered between two successive electron collisions along the period T_w of the microwave. Therefore, the calculations become impractical for large values of N_s, which depends on the available computational resources and was fixed at $N_s = 200$ in this case.

This maximum value N_s for the number of electron collisions during T_w introduces an upper bound for the gas pressure $p_a \sim \nu_m$ in the simulations. The maximum allowed pressures of argon represented in Fig. 2 depend on N_s, the

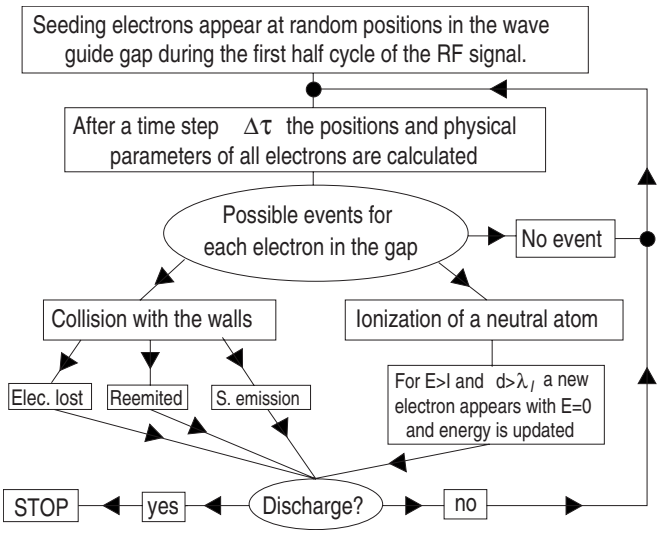

FIG. 3. Structure of the numerical simulations.

momentum transfer cross section σ_m, the microwave peak amplitude V_o, and the microwave frequency f_w.

For p_a exceeding the limits of Fig. 2, the friction force dominates, and the motion of electrons is limited by collisions. The high rf electric field continuously increases the energy of the charged particles which are confined in the space considered. This collisional confinement of electrons leads to an unrealistic overestimation of the ionizing collisions.

The iterative scheme of the simulations is represented in Fig. 3. During the first half cycle of the rf wave, the initial electron population is distributed at random positions at the lower wall of Fig. 1. The energy spread of these Maxwellian electrons is characterized by an initial electron temperature $K_B T_e$.

The dimensionless position and velocity of the electrons are calculated after an small time step $\Delta\tau$, and the possible events are considered for each of present particles: the electron motion may continue, driven by the rf electric field; the collisional ionization of a neutral atom occurs; or the electron may eventually impact the surfaces.

As indicated in Fig. 1, those electrons hitting the walls can be absorbed, re-emitted, or produce a new electron by secondary electron emission [12]. In order to determine the occurrence of a collisional ionization event, two conditions are checked for each dimensionless time step $\Delta\tau$. First is that the electron kinetic energy is above the first ionization energy $E > E_I$ of the neutral gas. On the other hand, the length L_I that the electron travels after its last ionizing collision must be larger than the ionization mean-free path $\lambda_I < L_I$.

When both conditions are met, an electron impact ionization occurs and a secondary electron is introduced in the simulation placed at this point. The length L_I of both electrons is reset, and the kinetic energy of the primary electron is reduced by an amount E_I. After the collision event, the velocity of the primary electron points to a random direction and both electrons move in the next time step $\Delta\tau$. The kinetic energy of the secondary electron is negligible compared with the large energy acquired from the microwave electric field in this time step.

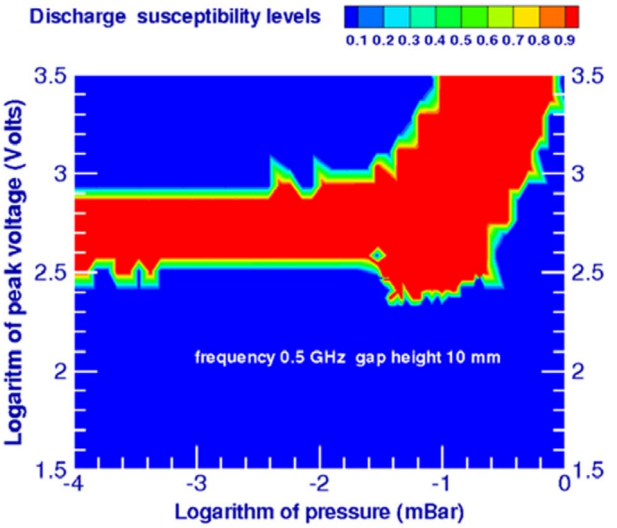

FIG. 4. (Color online) The predicted rf breakdown voltage thresholds corresponding to the experiments of Ref. [17] for different gas pressures. The decimal logarithm is used in both axes.

Finally, we calculate a qualitative measure that we call susceptibility, which accounts for the rate of electron production with respect to the dimensionless time,

$$H(\tau) = \frac{d}{d\tau}\ln[N_e(\tau)],$$

where $N_e(\tau)$ is the number of electrons present in the simulation. For a constant or decreasing electron population $H(\tau) \leq 0$, while it is positive when the electron multiplication takes place. This quantity is numerically approximated by

$$H(\tau + \Delta\tau) \simeq \frac{1}{\Delta\tau}\ln\left(\frac{N_e(\tau + \Delta\tau)}{N_e(\tau)}\right).$$

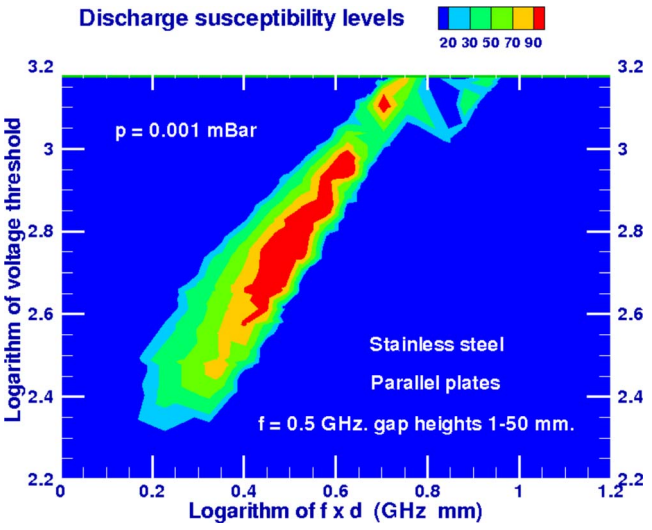

FIG. 5. (Color online) The rf voltage thresholds as a function of $f_w D$ for the low pressure electron multipactor. The decimal logarithm is employed in both axes.

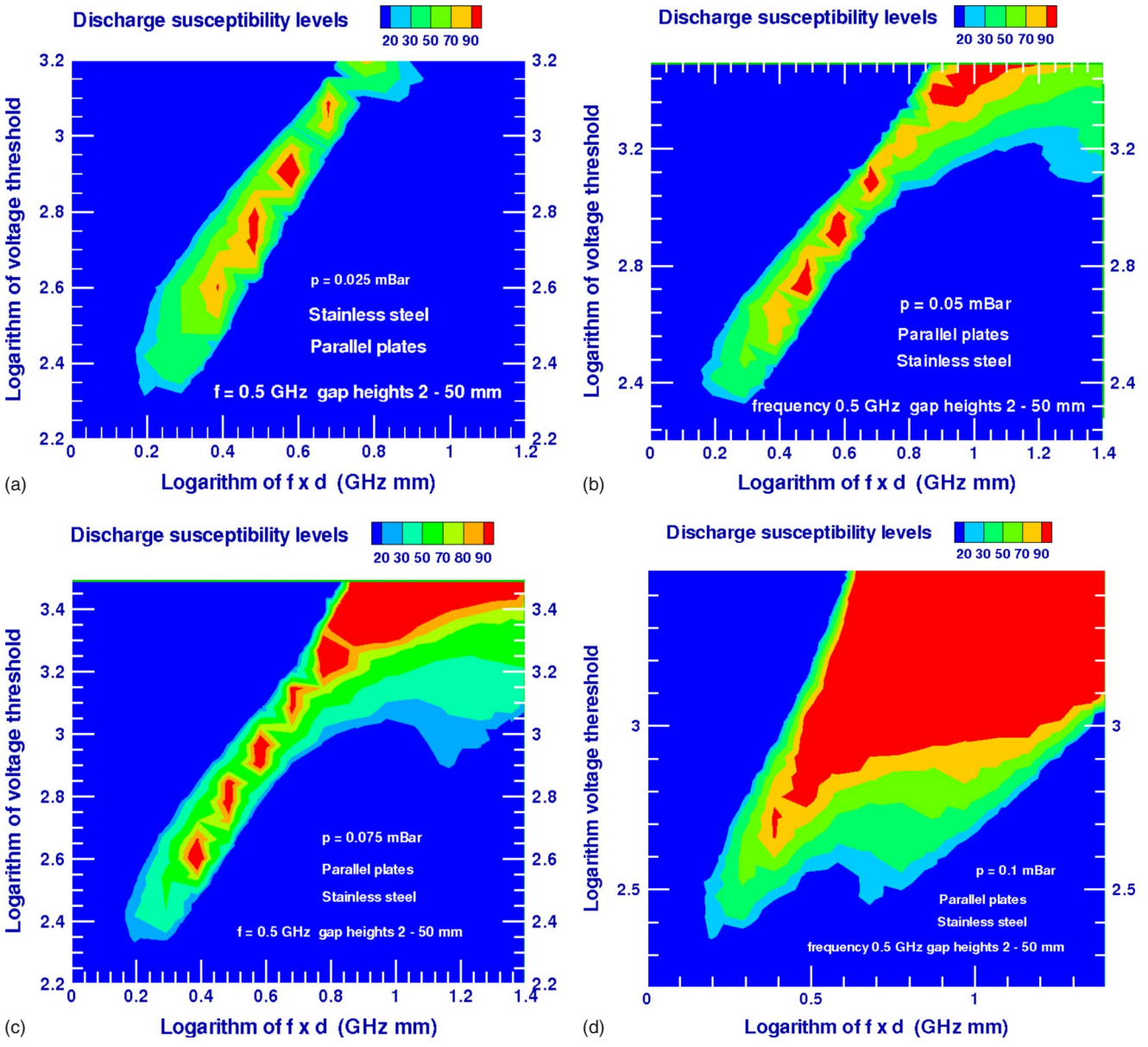

FIG. 6. (Color online) The rf voltage thresholds for rf breakdown in argon as a function of $f_w D$ for different values of the ratio ν_m/f_w within the collisional multipactor plasma range of pressures. The decimal logarithm is employed in all axes.

The final value of $H(\tau)$ is recorded when the simulation stops, and its magnitude is represented by means of a color code. This occurs when $N_e(\tau)$ reaches its maximum allowed value or when the characteristic time T_d is elapsed. Otherwise, as shown in Fig. 1, all the parameters are calculated again and a new integration step of Eqs. (3.6)–(3.8) is performed.

V. NUMERICAL RESULTS

Figure 4 represents the rf breakdown peak voltages as a function of the neutral gas pressure for argon, which are in agreement with the experimental results of Ref. [17]. The constant gap height was $D=10$ mm, the microwave frequency $f_w=0.5$ GHz, while the material at the parallel plates in Fig. 1 was stainless steel.

For low pressures, where $\nu_m/f_w \ll 1$ (typically below 10^{-3} mbar), the force acting on electrons in Eqs. (3.6)–(3.8) is essentially the rf electric field and therefore the results are equivalent to those of low pressure multipactor. The new electrons are produced by secondary emission at the walls in Fig. 1. Thus, the high and the low voltage thresholds for the rf breakdown in Fig. 4 are related to the two crossover energies of the secondary emission yield [4–7,12].

Figure 5 represents the MP breakdown voltages for a fixed pressure of $p_a=1.0\times10^{-3}$ mbar against the product $f_w D$. In these calculations $4.3\times10^{-2}\leq\nu_m/f_w\leq0.12$ and the electron impact ionization is negligible. These results are in agreement with previous experimental and theoretical results for the pure electron multipactor [12].

The electron impact ionization of neutral gas atoms increases with the gas pressure; Figs. 6 and 7 show the transi-

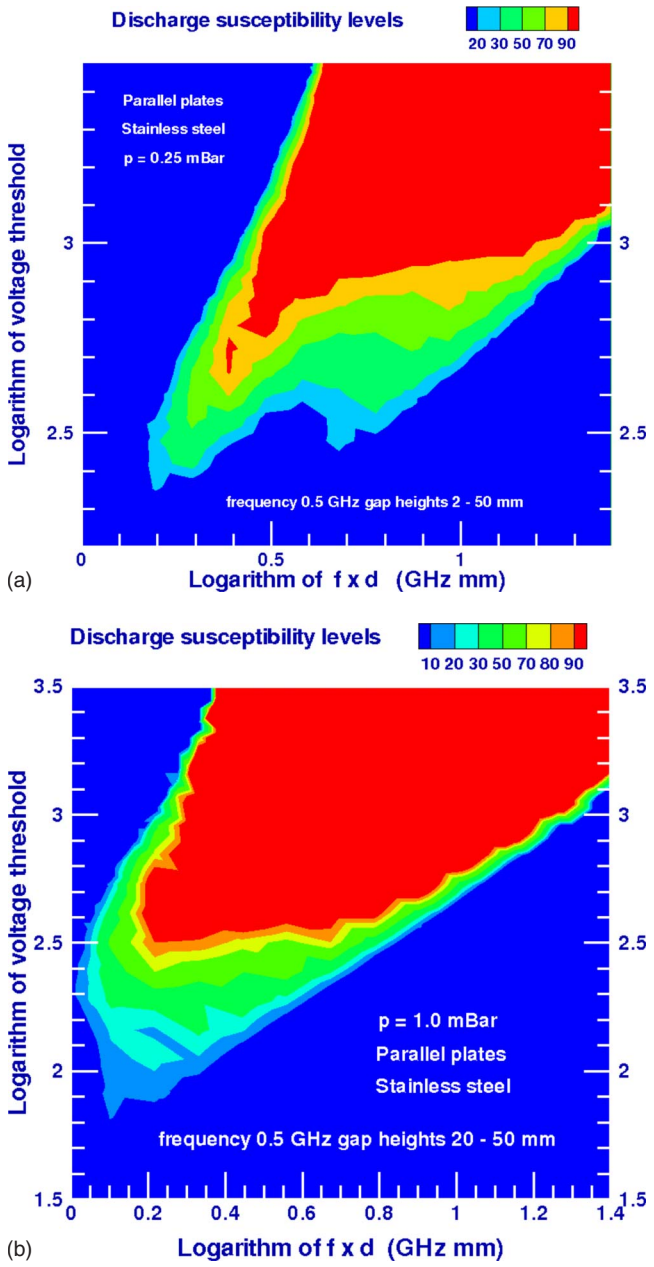

FIG. 7. (Color online) The rf voltage thresholds for rf breakdown as a function of f_wD for large values of the ratio ν_m/f_w. The decimal logarithm is employed in both axes.

tion from MP to collisional multipactor. In these calculations, the pressure is incremented from $p_a=2.5\times10^{-2}$ mbar up to $p_a=1.0$ mbar, and in consequence the ratio ν_m/f_w also grows.

The rf discharge zones of Figs. 6 and 7 become broader for similar microwave peak amplitudes V_o. The higher values for the susceptibility $H(\tau)$ indicate the faster growth of the electron population originated by the collisional ionization with p_a. Figures 6(d), 7(a), and 7(b) show that, for higher microwave peak amplitudes V_o and larger values of f_wD, the contribution of ionizing collisions to the electron production rate increases.

For a fixed microwave frequency the collisional ionization grows for higher values of the gap height D, because the energized electrons may experience a larger number of elastic and ionizing collisions. Equivalently, for a fixed value of D, the increments in the microwave frequency f_w confine the electrons because of the fast change in the direction of the wave electric field $\mathbf{E}_w(t)$. Therefore, the collisional electron production becomes more efficient for higher values of f_wD and V_o as the gas pressure p_a is increased.

VI. DISCUSSION AND CONCLUSIONS

The results of simulations shown in Figs. 4, 6, and 7 for the collisional multipactor and the electron multipactor are in agreement with experimental measurements for intermediate and low gas pressures [12,17]. However, our present model does not account for the hysteresis processes observed in the rf discharge thresholds in the experiments of Ref. [17]. For a fixed gas pressure, the rf discharge disappears for microwave amplitudes below the values for the start of the charge avalanche when the amplitude is incremented. This difference between the disappearance and breakdown rf amplitudes was observed for both the CMP and high pressure discharges and is related to the collisional ionization [17].

As evidenced in Fig. 2, the Langevin simulations are efficient for typical gas pressures below 1 mbar, where the typical length D and the wave period T_w are of the same order than the mean-free path and characteristic collisional time. For gas pressures or rf frequencies $\nu_m \gg f_w$ over this weakly collisional regime, the simulations are impractical because of the long computational time required in the numerical calculations to reproduce the random motion of electrons using Eq. (3.5).

In consequence, the minimum rf breakdown voltage predicted by the Paschen curves may be reproduced only when the corresponding gas pressure lies within the limits for the numerical calculations shown in Fig. 2. This minimum voltage for the charge avalanche is close to the transition to the drift diffusion regime where the average displacement of electrons is limited [28].

The minimum breakdown voltage in Fig. 4 corresponds to the pressure where $(p_aD)_{\min}\simeq0.1$ mbar cm. This is in agreement with the results of Ref. [17] and is similar to the experimental and the theoretical values $(p_aD)_{\min}\simeq0.4$ mbar cm in Ref. [28]. However, the magnitude of the predicted discharge voltage is higher by a factor of 2. The experiments evidence that the left-hand branch of the Paschen curve is strongly dependent on the secondary electron emission characteristics of electrodes [28], and this discrepancy would be related to the different surface properties and energy yields for the secondary electron emission.

The rf charge avalanche requires electron energies on the order of tens of electron volts and the involved microwave amplitudes are large. Therefore, only a small fraction of the electrons present in the simulation have energies below the ionization threshold along the period T_w of the microwave. In consequence, the contribution of low-energy effects in the cross section for elastic collisions is negligible. This would explain why the constant collision frequency model leads to acceptable results in Figs. 4, 6, and 7.

The main drawback for our present simulations is in the simplified model employed for the collisional ionization,

which is inefficient for gas pressures where collisions $\nu_m \gg f_w$ are dominant. This large number of elastic collisions hinder the electron displacements, leading to an average drift motion of electrons, which cover large distances within a restricted volume. The energy of these electrons becomes continuously incremented by the microwave electric field, while the collisional energy losses are not considered in Eq. (3.5). This combination of an increasing energy with the collisional confinement of electrons results in the overestimation of the number of ionizing collisions of electrons.

The PIC Montecarlo schemes, where the simulated particles consist of an aggregation of physical charges, are best suited for the simulation at high pressures or fully developed plasmas. This statistical approach overcomes the restricted pressure range and the limited time scale of T_d by considering the charge space effects [21,28]. On the contrary, the details of electron impacts at the walls and the actual secondary electron emission production rate are blurred up.

Figures 4, 6, and 7 shown that this individual particle model reproduces the low pressure MP and the intermediate pressure range for CMP. The Langevin simulations are efficient when the charge production at the walls dominates, or its contribution is of the same order than the electron impact ionization.

ACKNOWLEDGMENTS

The authors are grateful to Professor J. M. Donoso and Dr. C. Miquel for stimulating discussions. This work was supported by ESA-ESTEC under Program No. AO 4025 ITT ESA "Surface treatment and coating for the reduction of multipactor and passive intermodulation (PIM) effects in RF components" and by Ministerio de Ciencia e Innovación of Spain under Grant No. ENE-2007-67406-C02-01. The support from Tesat-Spacecom GmbH and fruitful discussions with D. Wolk, A. Meinrad, and U. Wolchner are also gratefully acknowledged.

[1] A. B. Filuk, J. E. Bailey, M. E. Cuneo, P. W. Lake, T. J. Nash, D. D. Noack, and Y. Maron, Phys. Rev. E **62**, 8485 (2000).
[2] A. Hassanein, Z. Insepov, J. Norem, A. Moretti, Z. Qian, A. Bross, Y. Torun, R. Rimmer, D. Li, M. Zisman, D. N. Seidman, and K. E. Yoon, Phys. Rev. ST Accel. Beams **9**, 062001 (2006).
[3] M. Farahmand, M. Weber, L. Tirino, K. F. Brennan, and P. P. Ruden, J. Phys.: Condens. Matter **13**, 10477 (2001).
[4] R. A. Kishek, Y. Y. Lau, L. K. Ang, A. Valfells, and R. M. Gilgenbach, Phys. Plasmas **5**, 2120 (1998).
[5] J. R. M. Vaughan, IEEE Trans. Electron Devices **35**, 1172 (1988).
[6] A. J. Hatch and H. B. Williams, Phys. Rev. **112**, 681 (1958).
[7] V. Semenov, A. Kryazhev, D. Anderson, and M. Lisak, Phys. Plasmas **8**, 5034 (2001); A. Sazontov, M. Buyanova, V. Semenov, E. Rakova, N. Vdovicheva, D. Anderson, M. Lisak, J. Puech, and L. Lapierre, *ibid.* **12**, 053102 (2005).
[8] G. Torregrosa, A. Coves, C. P. Vicente, A. M. Pérez, B. Gimeno, and V. Boria, IEEE Electron Device Lett. **27**, 619 (2006).
[9] L. Wu and L. K. Ang, Phys. Plasmas **14**, 013105 (2007).
[10] A. Valfells, J. P. Verboncoeur, and Y. Y. Lau, IEEE Trans. Plasma Sci. **28**, 529 (2000).
[11] H. C. Kim and J. P. Verboncoeur, Phys. Plasmas **12**, 123504 (2005).
[12] J. de Lara, F. Pérez, M. Alfonseca, L. Galán, I. Montero, E. Román, and D. Raboso, IEEE Trans. Plasma Sci. **34**, 476 (2006); F. Pérez, J. de Lara, L. Conde, M. Alfonseca, L. Galán, and D. Raboso, Simul. Model. Pract. Theory **16**, 1438 (2008).
[13] Y. P. Raizer, *Gas Discharge Physics* (Springer Verlag, Berlin, 1991), Chap. 7.
[14] A. E. D. Heylen and V. Postoyalko, Int. J. Electron. **71**, 707 (1991).
[15] M. Radmilović-Radjenović and J. K. Lee, Phys. Plasmas **12**, 063501 (2005); S. Roy and D. Gaitonde, J. Appl. Phys. **96**, 2476 (2004).
[16] V. I. Kobolov and R. R. Arsianbekov, IEEE Trans. Plasma Sci. **34**, 895 (2006).
[17] F. Höhn, W. Jacob, R. Beckmann, and R. Wilhem, Phys. Plasmas **4**, 940 (1997).
[18] R. Udiljak, D. Anderson, M. Lisak, V. E. Semenov, and J. Puech, Phys. Plasmas **10**, 4105 (2003).
[19] S. Riyopoulos, Phys. Plasmas **11**, 2036 (2004).
[20] R. Udiljak, D. Anderson, M. Lisak, V. E. Semenov, and J. Puech, Phys. Plasmas **11**, 5022 (2004).
[21] D. Vender, H. B. Smith, and R. W. Boswell, J. Appl. Phys. **80**, 4292 (1996).
[22] A. Gilardini, J. Phys. D **32**, 1281 (1999).
[23] W. M. Manheimer, M. Lampe, and G. Joyce, J. Comput. Phys. **128**, 553 (1997).
[24] B. J. Albright, D. Winske, D. S. Lemons, W. Daughton, and M. E. Jones, IEEE Trans. Plasma Sci. **31**, 19 (2003); M. E. Jones, D. S. Lemons, R. J. Mason, V. A. Thomas, and D. Winske, J. Comput. Phys. **123**, 169 (1996).
[25] J. Qiang and S. Habib, in *Proceedings of the 20th Linac Conference, Monterrey, California, 2000* (SLAC, Menlo Park, CA, 2000), pp. 89–91.
[26] B. J. P. Dowds, R. K. Barrett, and D. A. Diver, Phys. Rev. E **68**, 026412 (2003).
[27] L. E. Kline and J. G. Siambis, Phys. Rev. A **5**, 794 (1972).
[28] H. C. Smith, C. Charles, and R. W. Boswell, Phys. Plasmas **10**, 875 (2003).
[29] P. Felsenthal and J. M. Proud, Phys. Rev. **139**, A1796 (1965).
[30] A. G. Zhidkov, Phys. Plasmas **5**, 385 (1998).
[31] J. Dunkel, W. Ebeling, and S. A. Trigger, Phys. Rev. E **70**, 046406 (2004).
[32] D. J. Higham, SIAM Rev. **43**, 525 (2001).